Nuclear Instruments and Methods in Physics Research A 859 (2017) 31–36

Contents lists available at ScienceDirect

Nuclear Instruments and Methods in Physics Research A

journal homepage: www.elsevier.com/locate/nima

On the timing performance of thin planar silicon sensors

N. Akchurin[h,*], V. Ciriolo[g], E. Currás[a,b], J. Damgov[h], M. Fernández[b], C. Gallrapp[a], L. Gray[f], A. Junkes[c], M. Mannelli[a], K.H. Martin Kwok[i], P. Meridiani[e], M. Moll[a], S. Nourbakhsh[d], S. Pigazzini[g], C. Scharf[c], P. Silva[a], G. Steinbrueck[c], T. Tabarelli de Fatis[g], I. Vila[b]

[a] CERN, CH-1211 Geneva 23, Switzerland
[b] IFCA (CSIC-UC), E-39005 Santander, Cantabria, Spain
[c] Hamburg University, 20148 Hamburg, Germany
[d] University of Minnesota, School of Physics and Astronomy, Minneapolis, MN 55455, USA
[e] INFN Sezione di Roma, Roma, Italy
[f] Fermilab, Batavia, IL 60510, USA
[g] Università di Milano Bicocca and INFN Sezione di Milano-Bicocca, Piazza della Scienza 3, I-20126 Milano, Italy
[h] Texas Tech University, Department of Physics and Astronomy, Lubbock, TX 79409, USA
[i] Brown University, Department of Physics, Providence, RI 02912, USA

ARTICLE INFO

Keywords:
Silicon sensors
Time response
Calorimetry

ABSTRACT

We report on the signal timing capabilities of thin silicon sensors when traversed by multiple simultaneous minimum ionizing particles (MIP). Three different planar sensors, with depletion thicknesses 133, 211, and 285 μm, have been exposed to high energy muons and electrons at CERN. We describe signal shape and timing resolution measurements as well as the response of these devices as a function of the multiplicity of MIPs. We compare these measurements to simulations where possible. We achieve better than 20 ps timing resolution for signals larger than a few tens of MIPs.

1. Introduction

Event reconstruction at future hadron colliders will be challenged by the dramatic increase in the number of concurrent interactions (pileup) per beam crossing in the experiments. At the High-Luminosity Large Hadron Collider (HL-LHC) –with up to 200 pileup events per beam crossing–, current detectors will show limitations in the reliance on purely spatial information to resolve interactions and associate particles to vertices. Moreover, the random overlap of energy deposits from neutral particles, which cannot be associated via a track to any vertex, will deteriorate the calorimeter performance in terms of energy measurement and particle identification as particles appear to be less isolated. A compact and highly granular sampling calorimeter based on silicon sensor technology has been chosen to replace the end-cap calorimeter in the CMS experiment at the HL-LHC [1]. Precision time measurement of the energy deposits could provide an additional means to resolve interactions by exploiting the spread in the time domain of the collision vertices predicted to be about 150 ps RMS, within the 25 ns bunch crossing structure of the colliding beams at the HL-LHC [2].

The silicon trackers have played crucial roles in many experiments because they afford excellent spatial resolutions at high rates and are robust. There are also a handful of examples of sampling calorimeters based on active silicon sensors. The SICAPO collaboration studied salient features of electromagnetic calorimeters with layers of high-Z absorber and silicon sensors for what were then future colliders [3]. The ALEPH and OPAL collaborations employed luminosity calorimeters consisting of tungsten and silicon sensors [4,5]. The CALICE collaboration has been investigating high-granularity calorimeters with different types of active elements as well as silicon for precision physics at future colliders [6]. In recent times, silicon sensors have also been used for timing applications in high intensity environments. The NA62 Gigatracker is one example [7]. In a beam with a flux reaching 1.3 MHz/mm^2, they have achieved single-hit timing with 200 ps RMS resolution.

In this paper, we report on the results of our first study with small planar sensors with focus on their precision timing capability, in particular for the case of multiple particles impinging simultaneously on the sensors. The shower develops extremely rapidly to be considered simultaneous: for example, the simulation suggests ~0.16 ps RMS in shower development time for 50 GeV electrons in 4 X_o absorber. We briefly describe the experimental setup in Section 2 and discuss the pulse shape reconstruction and single minimum ionizing particle (MIP)

* Corresponding author.
E-mail address: Nural.Akchurin@ttu.edu (N. Akchurin).

http://dx.doi.org/10.1016/j.nima.2017.03.065
Received 26 August 2016; Received in revised form 28 February 2017; Accepted 29 March 2017
Available online 04 April 2017

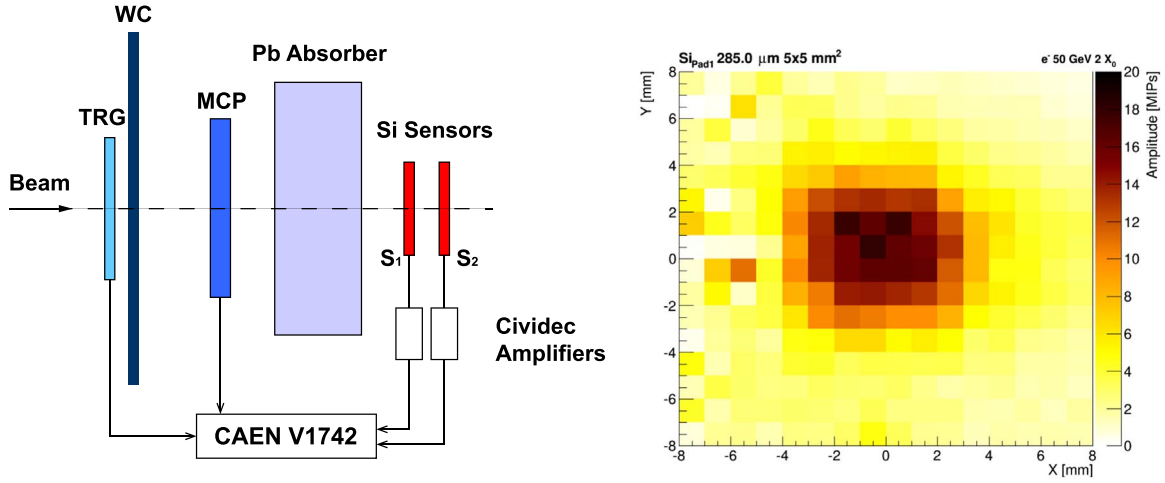

Fig. 1. The schematic of the layout displays the main components and the readout scheme on the left. Downstream of the trigger counter (TRG) and wire chambers (WC), a micro-channel plate (MCP) photomultiplier tube was positioned to provide a timing reference in front of the silicon sensors. Various lead plates were placed in between the MCP and the sensors to evaluate their response to multi-MIPs. A typical response pattern of a 285-µm thick silicon sensor (5×5 mm^2) to 50 GeV electrons when normalized to the MIP signal is displayed on the right. Note that the sensors were placed behind $2X_0$ of lead absorber in this case.

calibration in Section 3. We present multi-MIP response of the sensors in Section 4 and evaluate the timing resolution in Section 5 in some detail.

2. Experimental setup

The test setup is shown in Fig. 1. Two silicon sensors were installed in the beam line at all times. A micro-channel plate (MCP), viewing a Cherenkov radiator, provided a precise timing reference for each event within ~20 ps, with full efficiency for single MIPs at −2750 V [8]. A scintillator counter (2×2 cm^2) upstream of the detectors defined the area of triggered events. The impact position of particles on the sensors was estimated by projecting the hit positions, with better than a millimeter resolution, obtained from a set of delay wire chambers (Fig. 1). Lead sheets with different thickness were positioned in front of the sensors to generate electromagnetic showers to be able to investigate the multi-MIP response of these sensors.

The measurements described in this paper were performed at the H2 beam line of the super proton synchrotron (SPS) at CERN in July 2015. 150 GeV muons and 50 GeV electrons were used for the majority of the measurements. The beam particle intensities were typically several thousand per spill. Each spill lasted 4.9 s and was repeated twice a minute for most of the data taking period. Although the beam spot size on the sensors varied slightly with the beam tune and settings, the FWHM was about 1 cm in horizontal and vertical directions – larger than the sensors (Fig. 1).

All tested sensors were p-type (n-on-p), 5×5 mm^2 in the effective area and physically 32. µm thick. They were biased at 600 V and fully depleted. They were produced by deep-diffused float-zone (dd-FZ) technique by Hamamatsu within the framework of the CMS tracker upgrade project in three different depletion thickness: 133, 211, and 285 µm with capacitances of 22.5, 13.6, and 9.9 pF, respectively [9,10]. The radiation effects on these sensors are currently under study; however, none of the sensors used here was previously irradiated.

The electrical signals from the sensors were amplified by a broad-band (2 GHz/40 dB) amplifier,[1] and the waveforms were digitized at 5 GHz by a Domino Ring Sampler (DRS) unit from CAEN (V1742). The signals from MCP and the event trigger were also fed to the same digitizer unit in order to remove trigger jitter off-line. The intrinsic timing resolution of the digitizer was ~5 ps and did not contribute to the systematic uncertainty of our measurements in any significant way [11].

3. Pulse shape and MIP calibration

The rise-times from 10% to 90% of the pulse amplitude for the three sensors were measured to be 1.1 ns (Fig. 2). The pulse time was defined as the time when the pulse reaches its 50% amplitude. The offline algorithm searched for a pulse in the data stream, fitted its peak with a Gaussian function requiring at least 5 samples, and calculated the time at which the pulse reached its half amplitude.

We measured the responses of the three different type of sensors to single MIPs. A 50 GeV electron beam was used to perform this measurement. Without the lead plates in front of the sensors, 50 GeV electrons were effectively equivalent to MIPs. The results of the calibration with electrons have been found to be in agreement with the ones obtained using a 150 GeV muon beam. We selected events with a signal from the MCP and from the second sensor. The presence of a signal in the second sensor ensured that most tracks did pass through the first sensor whose response was being measured. The signal from the first sensor included a correction for a 20% noise

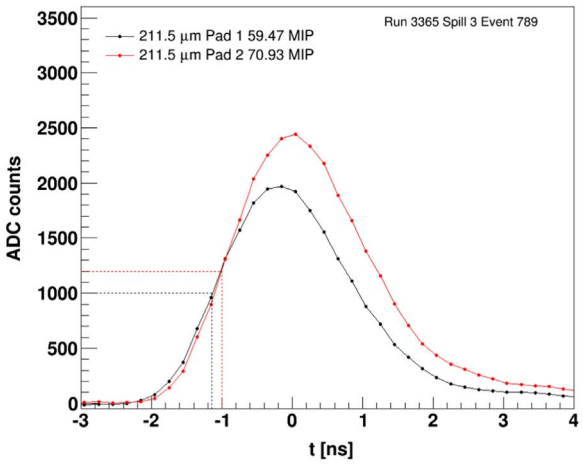

Fig. 2. Examples of single pulse shapes from two 211-µm thick sensors for the same event are shown on the left. 50% of the peak amplitude is indicated by dotted lines and is used in all the timing measurements discussed in Section 5. The peak of the pulses is arbitrarily set at t=0.

[1] CIVIDEC Instrumentation, C2 Broadband Diamond Amplifier, Vienna, Austria.

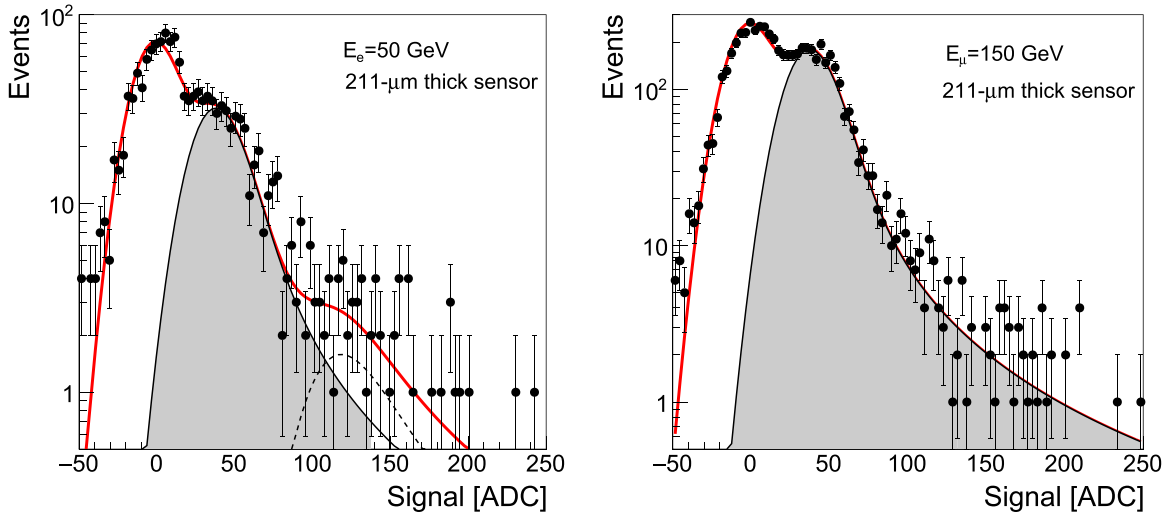

Fig. 3. The response of a 211-μm thick sensor to 50 GeV electrons (left): the red solid line depicts the fitted curve, which includes a Gaussian (pedestal centered around zero) and two Landau distributions convoluted with Gaussian distributions accounting for one (gray area) and three (dashed line) charged particles traversing the sensors. The distribution on the right is the same but for 150 GeV muons. Note the absence of events due to more than one charged track in this case. (For interpretation of the references to color in this figure legend, the reader is referred to the web version of this article.)

correlation between the two sensors. The major sources of the noise correlations come from the amplifier power supply line and the common noise in the digitizer inputs. The signal distribution from the first sensor included contributions from zero (e.g. no signal) and single-track (1 MIP) events, as well as from a small number of events with 3 charged tracks (3 MIPs) where a photon emitted by the interacting initial electron produced an electron-positron pair. We modeled this spectrum with a linear sum of a Gaussian and two Landau distributions convolved with a Gaussian distribution, representing contributions from 1 MIP and 3 MIPs. Fig. 3 shows the signal distributions. The most probable value (MPV) of the Landau distribution establishes the MIP measurement. The precision of the measurement was limited by the amount of data and by the systematic uncertainties related to the noise correlation between the two sensors.

The MIP response of the three sensor thicknesses is compared in Fig. 4. The signal amplitude is plotted against the depletion zone thickness. We compare the MPVs (solid black squares) for each sensor for a MIP as well as for the signal-to-noise ratios (open red circles). The apparent increase in amplitude with sensor thickness is due to the decrease of the sensor capacitance rather than the increase in sensor current with a corresponding improvement in signal-to-noise ratio.

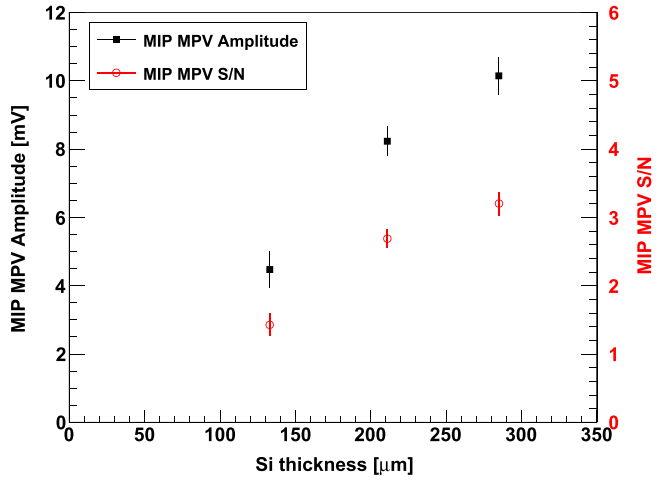

Fig. 4. Comparison of the sensor responses to MIPs as a function of their depletion-zone thickness. In open red circles, the signal-to-noise ratio for single MIPs are given (right scale). (For interpretation of the references to color in this figure legend, the reader is referred to the web version of this article.)

4. Multiple MIP signal

While clearly separated single-MIP response from the background is desirable and may be used to set the energy scale in calorimetry, measurement of the sensor response to multiple MIPs gives us a sense for response linearity. We consider a signal from 1, …, N tracks simultaneously passing through the silicon sensor, where N is small enough so the signals from different track multiplicities are distinguishable. In the absence of independent information providing the number of charged particles passing through the sensor, this study was particularly well-suited for our setup. Thus, we analyzed the spectrum containing events with different track multiplicities. We modeled the observed spectrum with an analytic function and then evaluated the linearity of the response from the parameters of this function. This procedure was also validated with a GEANT4 [12] simulation.

Two radiation lengths of lead were placed in front of the sensors with a 50 GeV electron beam initiating electromagnetic showers. We also required a signal from the MCP to ensure proper timing/jitter correction in signal reconstruction, as noted earlier.

The signal distribution was fitted with an analytic function (Fig. 5) with multiple components. Each component comprised a Landau distribution to describe ionization loss by a charged particle in a thin silicon layer convolved with a Gaussian distribution to model electronics noise. $N+1$ components were added linearly to describe a spectrum with track multiplicities ranging from 1 to N. The pedestal component of the distribution (no charged particle going through the sensor) was modeled by a Gaussian distribution, and its width was used to constrain the Gaussian component in the MIP signals. The only constraint in the fitting procedure was that the widths of the individual distributions were limited to a range. All other parameters were left free in the minimization process.

In order to evaluate the linearity of response, shown in Fig. 6, we formed a ratio of the MPVs of the Landau distributions from the measurements and simulations and found that for $N < 4$, the signal linearity was within 3–4% for the 285-μm-thick sensor.

5. Timing resolution

Fig. 7 depicts distributions of time differences between the first (S_1) and the second (S_2) sensors for three different sensors (133, 211, and 285 μm thick) and three ranges of signal ($3 < S_1$ and $S_2 < 8$ MIPs; $8 < S_1$ and $S_2 < 20$ MIPs; and $S_1 > 20$ and $S_2 > 20$ MIPs). The timing resolu-

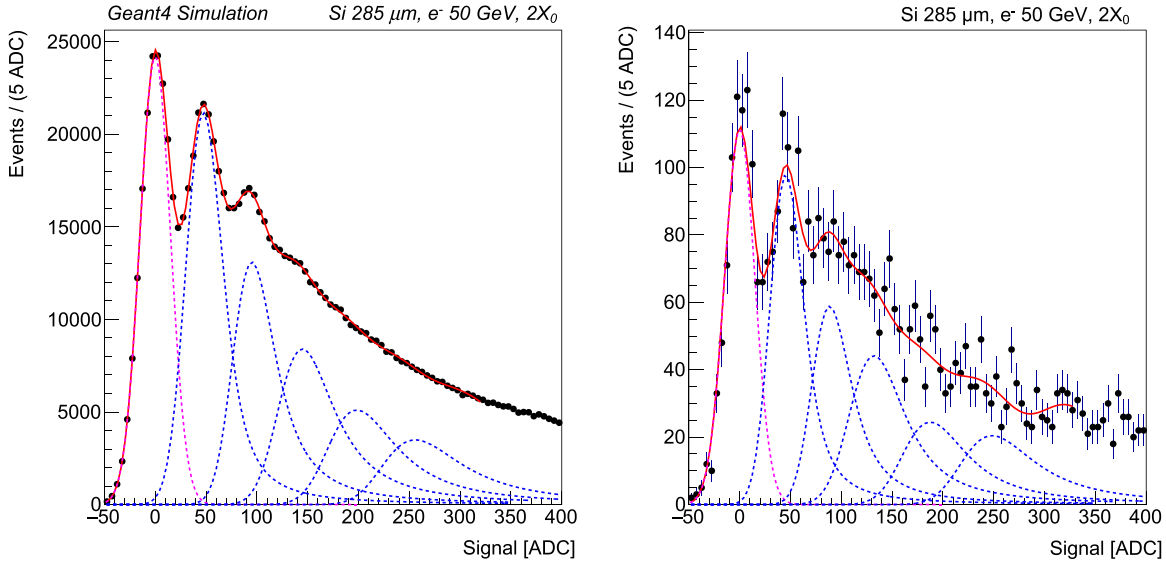

Fig. 5. Reconstructed multi-MIP signal from the GEANT4 simulation (left) and the beam data (right). The pedestal distributions are indicated by red dotted lines and centered at zero. The error bars are statistical only. (For interpretation of the references to color in this figure legend, the reader is referred to the web version of this article.)

tions are determined from the standard deviations resulting from the Gaussian fits to these distributions. This difference is divided by $\sqrt{2}$ because the two measurements are assumed to be equal and completely independent. For large signals ($S_1 > 20$ and $S_2 > 20$ MIPs), the timing resolution is better than 20 ps for all sensors. In the intermediate range ($8 < S_1$ and $S_2 < 20$ MIPs), the timing resolution varies from 30 to 60 ps, and when we require only a few MIPs ($3 < S_1$ and $S_2 < 8$ MIPs), the performance degrades significantly from 70 to 150 ps.

We evaluated the timing resolution performance of silicon sensors in three different combinations. The first measurement (I) was carried out using a pair of same-thickness silicon sensors as described above. For the second measurement (II), one silicon sensor was used in conjunction with an MCP. In the third measurement (III), we used the average of signals from two same-thickness silicon sensors and the signal from the same MCP as in the previous case. The results from each measurement are summarized in Table 1.

Measurement I: Fig. 8 presents the timing resolution as a function of the effective signal amplitude in units of MIPs and the effective signal-to-noise ratio. We defined the effective signal strength as $S_{\text{eff}} = S_1 S_2/\sqrt{S_1^2 + S_2^2}$. It can be seen that the timing performance improves with increasing signal strength (Fig. 8-left), but that for equal S_{eff}/N the timing performance of the three sensor types is similar (Fig. 8-right). The solid lines in Fig. 8 represent the fits to a form

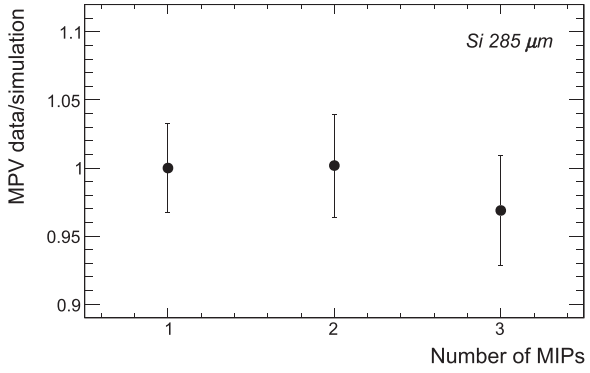

Fig. 6. The linearity of response to multiple charged tracks as a function of track multiplicity is within 3–4% in this narrow range. The vertical axis is the ratio of MPVs from the experimental data and simulations for the 285-μm thick sensor. The error bars are largely statistical because we measure a differential non-linearity with respect to one MIP where most of the systematic uncertainties cancel.

$$\frac{\sigma(t_1 - t_2)}{\sqrt{2}} = \frac{A}{\sqrt{2}S_{\text{eff}}} \oplus C \tag{1}$$

to quantify the timing resolution of the two-sensor system where A represents the 'noise' and C represents the 'constant' terms. The two

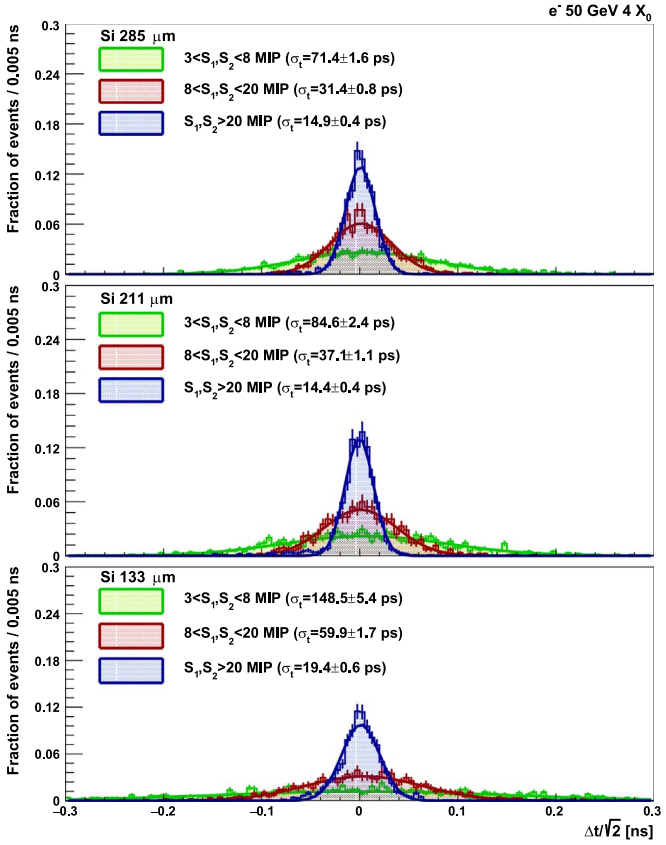

Fig. 7. The distribution of the time difference between the signals from a pair of silicon sensors ($\Delta t = t_1 - t_2$), 133-μm (bottom), 211-μm (middle), and 285-μm (top) thick, as a function of three different signal ranges as indicated on the upper left corner of each plot. The solid lines represent Gaussian fits to the data points. The sensors were placed behind a $4X_0$ lead absorber and the electron beam energy was 50 GeV.

Table 1
The summary of timing resolutions achieved by combinations of detectors are shown for three different cases. The first and second column indicate which two detectors are used in the measurement. In *Measurement III*, the average of the timing information from the two indicated silicon sensors is treated as the effective first detector, and the MCP as the second. The mean time is defined as $t_{\text{mean}} = \frac{1}{2}(t_{S1} + t_{S2})$. The errors on A and C are statistical and derived from fits.

Det 1	Det 2	Fit Function	A [ns×ADC]	C [ns]
Measurement I				
S_1(133-μm)	S_2(133-μm)	$\frac{\sigma(t_1 - t_2)}{\sqrt{2}} = \frac{A}{\sqrt{2}S_{\text{eff}}} \oplus C$	0.69 ± 0.01	0.010 ± 0.001
S_1(211-μm)	S_2(211-μm)		0.38 ± 0.01	0.009 ± 0.001
S_1(285-μm)	S_2(285-μm)		0.34 ± 0.01	0.010 ± 0.001
Measurement II				
S_1(133-μm)	MCP	$\sigma(t_1 - t_{\text{MCP}}) = \frac{A}{S_1} \oplus C$	0.62 ± 0.01	0.018 ± 0.001
S_1(211-μm)	MCP		0.40 ± 0.01	0.022 ± 0.001
S_1(285-μm)	MCP		0.35 ± 0.01	0.024 ± 0.001
Measurement III				
S_1(133-μm), S_2(133-μm)	MCP	$\sigma(t_{\text{mean}} - t_{\text{MCP}}) = \frac{A}{2S_{\text{eff}}} \oplus C$	0.75 ± 0.01	0.020 ± 0.001
S_1(211-μm), S_2(211-μm)	MCP		0.38 ± 0.01	0.019 ± 0.001
S_1(285-μm), S_2(285-μm)	MCP		0.33 ± 0.01	0.021 ± 0.001

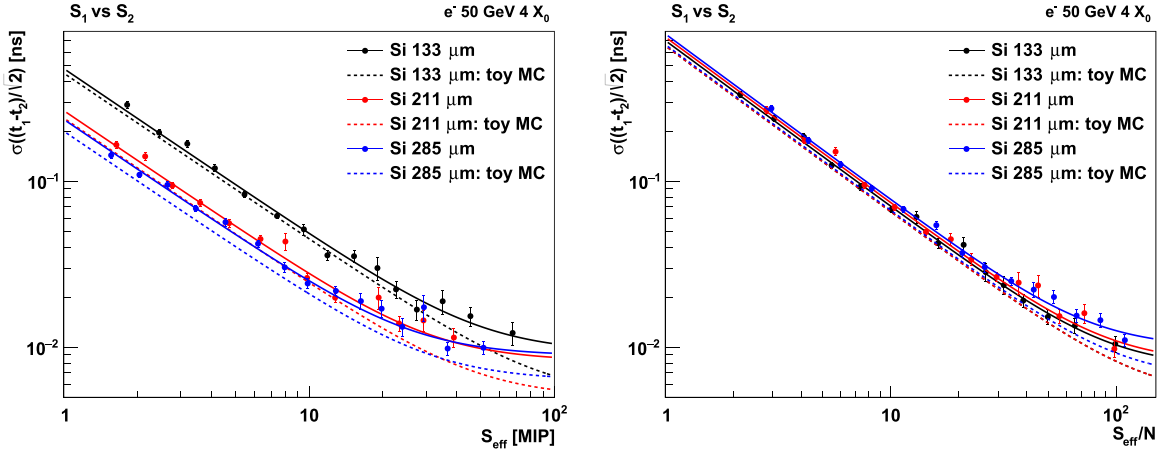

Fig. 8. The timing resolution based on two silicon sensors as a function of the effective signal strength in units of MIPs (left) and as a function of the signal-to-noise ratio (right). The fitted resolution functions with a noise (A) and a constant term (C) are also shown as solid lines. The dashed lines represent toy simulation results (see text for details).

terms on the right side of Eq. (1) are summed in quadrature as symbolized by ⊕, and the $\sqrt{2}$ factor accounts for the two independent sensors. When the signal strength is large, $S_{\text{eff}} \geq 80$ MIPs, the constant term dominates, and the timing resolution is about 10 ps. The toy simulation results are also plotted in Fig. 8 as dotted lines. This simulation was performed by using the average pulse shapes for each sensor and adding a Gaussian noise corresponding to the measured noise level. No noise correlation was introduced among the samples.

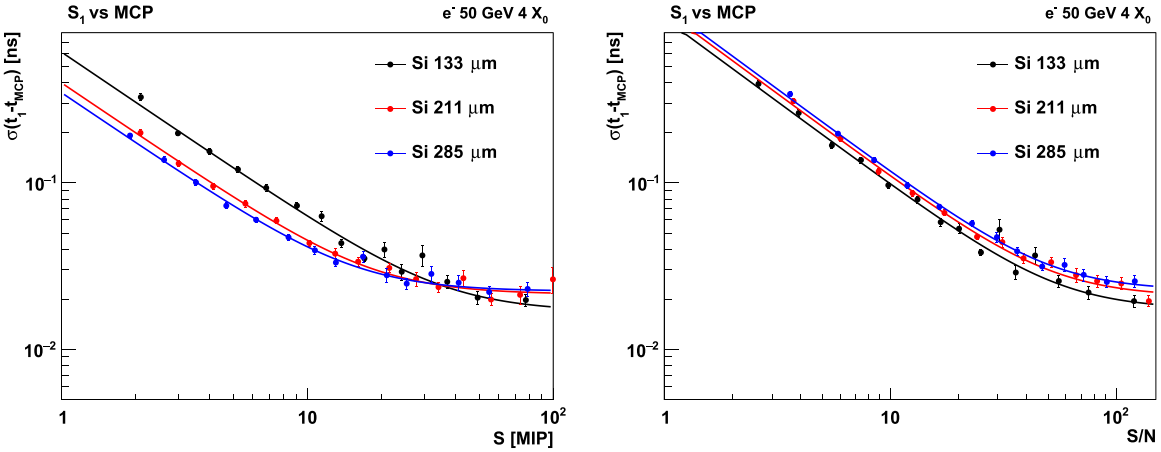

Fig. 9. The timing resolution between the first silicon sensor and the MCP as a function of the signal (left) and as a function of the signal-to-noise ratio (right). All three different thickness sensors are compared. The constant term, C, is dominated by the MCP resolution, estimated to be 21 ps.

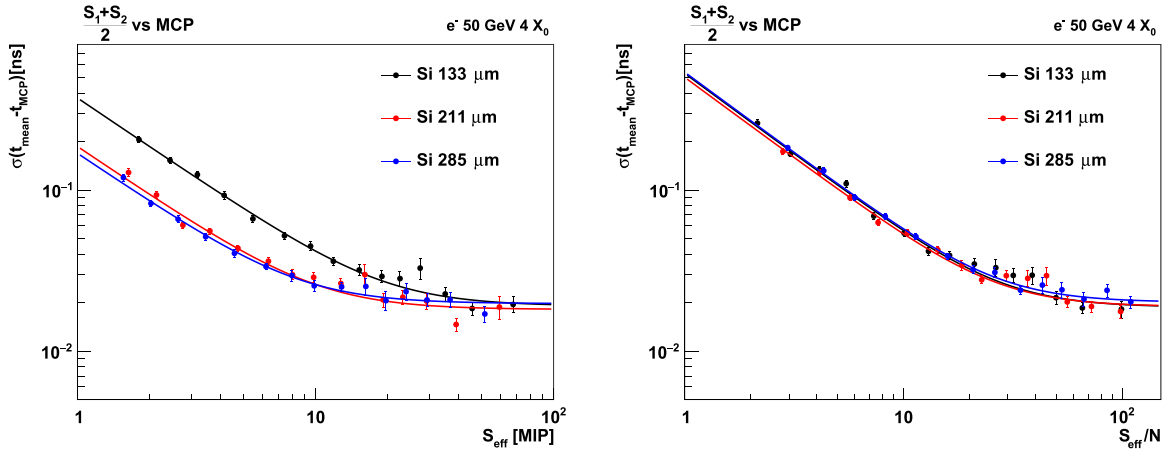

Fig. 10. The timing resolution between the mean signal of the two silicon sensors and the MCP as a function of the effective signal (left) and as a function of the signal-to-noise ratio (right).

The overall 'noise' terms are well reproduced in this way whereas the 'constant' term is underestimated, mainly because only 5 ps timing uncertainty contribution from the V1742 digitizer is accounted for in this simulation.

Measurement II: When the timing resolution was evaluated with one silicon sensor and an MCP, $\sigma(t_1 - t_{\mathrm{MCP}})$, the constant term varied from 18 to 24 ps reflecting the limiting performance of the MCP at large signals as shown in Fig. 9.

Measurement III: We also studied the average signal from two same-thickness silicon sensors versus the signal from the MCP, $\sigma(t_{\mathrm{mean}} - t_{\mathrm{MCP}})$. In this case (Fig. 10), the timing resolution of the system was dominated by that of the MCP as in *Measurement II*. However, the comparison of the noise terms reveals the potential power of the independent timing measurements from multiple silicon sensors. The noise term is a factor of $\sqrt{2}$ better than single sensor measurements (i.e in comparing with *Measurement I*).

6. Conclusions

In this study, we have shown that it is possible to perform precise timing measurements ($O(20)$ ps) using silicon sensors for large pulse heights, $S/N \gtrsim 20$. We have also shown that it is possible to further improve the timing measurement when information from several sensors are combined. For example, the possibility of measuring with high precision the shower time evolution offers novel opportunities, in particular it could allow the separation of nearby showers beyond what is achievable from the spatial segmentation and precise time information associated with each reconstructed shower in calorimetry. These pieces of information have the potential to improve the calorimeter performance in very dense environments, such as the forward region of CMS during HL-LHC operation. In the wake of these measurements, similar timing studies exposing silicon sensors to multiple MIPs have recently also been performed at Fermilab [13].

Acknowledgements

We would like to thank CERN for support and making particle beams of highest quality available for this work.

References

[1] CMS Collaboration, Technical Proposal for the Phase-II Upgrade of the CMS Detector, Technical Report CERN-LHCC-2015-010. LHCC-P-008, CERN, Geneva, 2015.
[2] S. Fartoukh, Pile up management at the high-luminosity LHC and introduction to the crab-kissing concept, Phys. Rev. Spec. Top-Accel. Beams 17 (2014) 111001.
[3] E. Borchi, et al., Silicon sampling hadronic calorimetry: a tool for experiments at the next generation of colliders, Nucl. Instrum. Methods A279 (1989) 57–65.
[4] D. Bederede, et al., SICAL: a high precision silicon - tungsten luminosity calorimeter for ALEPH, Nucl. Instrum. Methods A365 (1995) 117–134.
[5] G. Abbiendi, et al., Precision luminosity for Z0 line shape measurements with a silicon tungsten calorimeter, Eur. Phys. J. C14 (2000) 373–425.
[6] F. Sefkow, A. White, K. Kawagoe, R. Pöschl, J. Repond, Experimental tests of particle flow calorimetry, Rev. Mod. Phys. 88 (2016) 015003.
[7] G.A. Rinella, D.A. Feito, R. Arcidiacono, C. Biino, S. Bonacini, A. Ceccucci, S. Chiozzi, E. C. Gil, A.C. Ramusino, J. Degrange, M. Fiorini, E. Gamberini, A. Gianoli, J. Kaplon, A. Kluge, A. Mapelli, F. Marchetto, E. Minucci, M. Morel, J. Noel, M. Noy, L. Perktold, M. Perrin-Terrin, P. Petagna, F. Petrucci, K. Poltorak, G. Romagnoli, G. Ruggiero, B. Velghe, H. Wahl, The {NA62} gigatracker, Nuclear Instruments and Methods in Physics Research Section A: Accelerators, Spectrometers, Detectors and Associated Equipment, 2016.
[8] L. Brianza, et al., Response of microchannel plates to single particles and to electromagnetic showers, Nucl. Instrum. Methods A797 (2015) 216–221.
[9] A. Dierlamm, Characterisation of silicon sensor materials and designs for the CMS Tracker Upgrade, Technical Report AIDA-CONF-2014-006, CERN, Geneva, 2012.
[10] E. Curras, M. Fernandez, C. Gallrapp, L. Gray, M. Mannelli, P. Meridiani, M. Moll, S. Nourbakhsh, C. Scharf, P. Silva, G. Steinbrueck, T.T. de Fatis, I. Vila, Radiation Hardness and Precision Timing Study of Silicon Detectors for the CMS High Granularity Calorimeter (HGC), Nucl. Instrum. Meth., 2016.
[11] CAEN, V1742: 32+2 Channel 12bit 5 GS/s Switched Capacitor Digitizer, 2015.
[12] S. Agostinelli, et al., GEANT4: a Simulation toolkit, Nucl. Instrum. Methods A506 (2003) 250–303.
[13] A. Apresyan, G. Bolla, A. Bornheim, H. Kim, S. Los, C. Pena, E. Ramberg, A. Ronzhin, M. Spiropulu, S. Xie, Test beam studies of silicon timing for use in calorimetry, Nucl. Instrum. Methods 825 (2016) 62–68.